Electron beam analysis induces Cl vacancy defects in a NaCl thin film

Khalid Quertite, Hanna Enriquez, Nicolas Trcera, Azzedine Bendounan, Andrew J Mayne, Gérald Dujardin, Abdallah El Kenz, Abdelilah Benyoussef, Yannick J Dappe, Abdelkader Kara, et al.

Electron beam analysis induces Cl vacancy defects in a NaCl thin film

Khalid Quertite[1,2,3*], Hanna Enriquez[1], Nicolas Trcera[2], Azzedine Bendounan[2], Andrew J. Mayne[1], Gérald Dujardin[1], Abdallah El kenz[3], Abdelilah Benyoussef[3,4], Yannick J. Dappe[5], Abdelkader Kara[6], and Hamid Oughaddou[1,7]

[1]Université Paris-Saclay, CNRS, Institut des Sciences Moléculaires d'Orsay (ISMO), Bât. 520, 91405 Orsay, France

[2]Synchrotron Soleil, L'Orme des Merisiers, Saint-Aubin, B.P. 48, 91192 Gif-sur-Yvette Cedex, France

[3]LaMCScI, Faculté des Sciences, Université Mohammed V - Agdal, 10100, Rabat, Morocco

[4]Hassan II Academy of Sciences and Technology, Rabat, Morocco

[5]Université Paris-Saclay, CEA, CNRS, SPEC, 91191 Gif-sur-Yvette Cedex, France

[6]Department of Physics, University of Central Florida, Orlando, FL 32816, USA

[7]Département de Physique, CY, Cergy Paris Université, 95031 Cergy-Pontoise Cedex, France

*Corresponding Authors : *E-mail : khalid.quertite@gmail.com*

Abstract

This work reports on the electron-induced modification of NaCl thin film grown on Ag(110). We show using low energy electron diffraction (LEED) that electron beam bombardment leads to desorption and formation of Cl vacancy defects on NaCl surface. The topographic structure of these defects is studied using scanning tunneling microscopy (STM) showing the Cl defects as depressions on the NaCl surface. Most of the observed defects are mono-atomic vacancies and are located on flat NaCl terraces. Auger electron spectroscopy confirms the effect of electron exposure on NaCl thin films showing Cl atoms desorption from the surface. Using density functional theory (DFT) taken into account the van der Waals dispersion interactions, we confirm the observed experimental STM measurements with STM simulation. Furthermore, Comparing the adsorption of defect free NaCl and defective NaCl monolayer on Ag(110) surfaces, we found an increase of the adhesion energy and the charge transfer between the NaCl film and the substrate due to the Cl vacancy. In details, the adhesion energy increases between the NaCl film and the metallic Ag substrate from 30.4 $meV\text{Å}^{-2}$ for the NaCl film without Cl vacancy and from 39.5 $meV\text{Å}^{-2}$ for NaCl film with a single Cl vacancy. The charge transfer from the NaCl film to the Ag substrate is enhanced when the vacancy is created, from 0.63e^- to 1.25e^-.

Keywords: two-dimensional materials, atomic vacancies, insulating surfaces, low temperature scanning tunneling microscopy, DFT calculation.

1. Introduction

Insulating films supported by metal surfaces are very important in numerous nanoscience applications. They have been used successfully as atomically controlled spacers to decouple the electronic structure of adsorbates from those of the metal substrate. This allows the study and enhancement of the intrinsic electronic properties of these adsorbates, which is an important step towards nanotechnology applications. Recent research confirms the decoupling effect of these films as they have been used in numerous experiments: to image individual molecular orbitals [1, 2], to manipulate single adatoms [3-4] and to isolate 2D nano-structures [5, 6]. Sodium chloride (NaCl) is an alkali-halide insulator with wideband gap (8.5 eV) and it is considered an excellent model system to conduct such experiments. Previous studies reported that NaCl ultra-thin insulating films can grow by epitaxy as flat islands on different metal surfaces such as Ag [7, 8], Cu [9, 10] and Au [11, 12]. Further benefits of using NaCl thin films as substrates is the ability to use electron excitation surface analysis techniques as the charging effect on these films is weak. This allows following and controlling the growth of these films during the experiment, which leads to a better surface characterization. As side effect, these techniques usually affect the ionic surface under investigation by probe-induced damage. Electron-stimulated desorption has been observed on NaCl bulk and surfaces when using low-energy electron diffraction (LEED), Auger electron spectroscopy (AES) and reflection high-energy electron diffraction (RHEED) methods [13-17]. This electron-simulated desorption has been attributed to the ejection of Cl ions, a process that is also used to form color centers in NaCl films [18]. The ejection of halogen ions results in the formation of Cl atomic vacancy defects on the NaCl surface. Finally, prolonged exposure of NaCl films to electron irradiation leads to layer dissociation and formation of a new sodium-based 2D structure [13, 14].

Atomic vacancies play a key role in electronic properties and chemical reactivity of materials [19-23]. For insulating surfaces, vacancies have been exploited to trap molecules [24] and nano-clusters [25]. Previous work shows that Cl vacancies in a NaCl layer on the Cu surface can be an interesting example to study the electron-phonon coupling between optical phonons and the localized vacancy state [26]. Recently, it has been shown that measuring the lifetime of the vacancy state of Cl vacancies can be used to determine the local thickness of the insulating NaCl layer [27].

In this work, we show the effect of electron irradiation on a monolayer (1 ML) NaCl thin film grown on the Ag(110) surface and we confirm the formation of chlorine vacancies due to electron exposure. STM and AES have been used to study the structural and chemical

modifications upon electron exposure of the NaCl film. AES spectra indicate Cl atoms desorption from the surface and STM images show the Cl defects as depressions on the NaCl layer. Using DFT calculations, we confirm the observed experimental STM measurements with STM simulation. In addition, Comparing the adsorption of defect free NaCl and defective NaCl monolayer on Ag(110) surfaces, we found an increase of the adhesion energy and the charge transfer between the NaCl film and the Ag substrate due to the Cl vacancy.

2. Experimental and computational details

All experiments were performed in ultra-high vacuum. The system, operating at a base pressure $< 10^{-10}$ mbar, is equipped with the standard tools for surface preparation and characterization, including an Auger electron spectroscopy (AES), a low-energy electron diffraction (LEED) and a scanning tunneling microscope (STM). The thin NaCl film is grown on a single crystal of Ag(110). Prior to NaCl deposition, the Ag(110) substrate was cleaned by several cycles of Ar+ ion sputtering followed by annealing up to 500°C. NaCl was deposited by sublimation from a solid source Knudsen cell at 520°C. During the deposition, the Ag substrate was kept at 140°C. Annealing the substrate increases the NaCl molecule diffusion, which allows larger NaCl islands to be obtained [8]. Calibration was achieved by monitoring the quantity of the NaCl deposited using a quartz microbalance. The AES/LEED experiments presented here were performed at room temperature, while STM topographies were taken at low temperature (~ 77 K). Electron irradiation was carried out using LEED on a 1 ML NaCl film just after sample preparation and prior to probing the surface with STM. The typical LEED characterization was performed at an energy of 48 eV for less than one minute to check the surface structure. Given that the reaction kinetics of the NaCl layer upon electron irradiation has a characteristic time constant of 100s [14], keeping the exposure time to <1 minute enables us to investigate the initial Cl vacancy formation before the onset of the larger scale surface evolution at longer times scales. To confirm the effect of LEED electron irradiation on the NaCl film, we performed a prolonged electron exposure with LEED at 63 eV for 10 min. Furthermore, we analyzed the sample with AES method to check the surface chemical composition before and after electron exposure.

Calculations were performed within Density Functional Theory using the VASP [28, 29] code (version 5.4.4) with the GGA-PBE functional [30], where the interaction between the valence electrons and ionic cores is described by the projector augmented wave (PAW) method [31,

32]. We have also performed calculations using the optB88 [33] functional which is a van der Walls implementation into VASP. Several investigations have shown that the OptB88 provides an overall good agreement with experimental results [34-38]. The energy cut-off is set to 350 eV. For all calculations, Monkhorst-Pack sampling [39] is used. For bulk calculations, a 14x14x14 grid is used while for surface calculations a 4x4x1 is used. The charge transfer following the adsorption has been computed using Bader method analysis [40] as implemented by Henkelman *et al*. [41] and the simulated STM images are obtained using the Tersoff-Hamann approach [42]. Our model system for NaCl/Ag(110) is built by placing one Cl atom on a top site of the Ag(110) surface, since it is known that this structure presents the most stable configuration with the highest adsorption energy and the largest distortion of the Ag surface top layers [8].

3. Results and discussion

3.1. Cl vacancy formation and its topographic signature

Figure 1.a shows the LEED pattern of clean Ag(110) surface with its rectangular symmetry (white rectangle). After deposition of 1 ML of NaCl at 140°C, the LEED pattern in **Figure 1.b** reveals a new (4×1) superstructure (yellow rectangle). This superstructure is due to the small mismatch between the Ag(110) and NaCl(100) surfaces, in which, along the Ag[1–10] direction $4\times a_{\mathrm{Ag[1-10]}}$ = 1.155 nm equals approximately $3\times a_{\mathrm{NaCl[011]}}$ = 1.196 nm. In the Ag[001] direction, the lattice parameter $a_{\mathrm{Ag[001]}}$ = 0.408 nm is close to $a_{\mathrm{NaCl[01-1]}}$ = 0.400 nm. In both directions, we found a lattice mismatch of 3.55% and 2.00% for Ag[1-10] and Ag[001], respectively. We observe that the NaCl ¾ diffraction spot along the Ag[1-10] is more intense in the LEED pattern which reflects the (1x1) structure of the NaCl(100) layer.

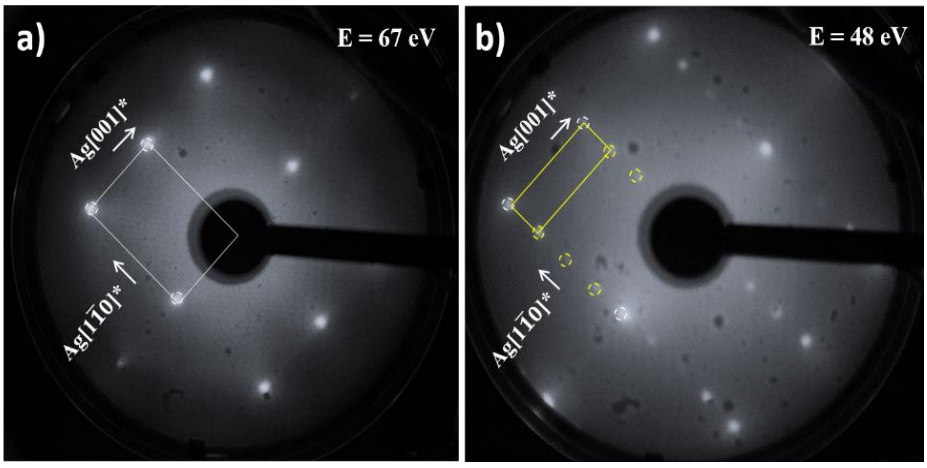

Figure 1. LEED patterns of (a) clean Ag(110) surface measured at 67 eV and (b) after a deposit of 1ML of NaCl measured at 48 eV. The white rectangle shows the (1x1) unit of Ag(110) while the yellow rectangle shows the (4x1) superstructure of NaCl/Ag(110).

The STM topographies were taken after performing a typical surface analysis with electron irradiation by LEED at 48 eV for less than 1 min. **Figure 2.a** presents STM topography of an ultra-thin NaCl film grown on Ag(110) at 140°C. The NaCl film consists in islands with an atomically flat surface and straight nonpolar edges, as well as a relatively important number of surface defects (mean density higher than 3 x 10^{18} cm^{-2}). A selection of point defects appearing on the NaCl film is shown with higher atomic resolution in **Figure 2.b**. Most of these defects were observed on flat NaCl terraces and not along step edges or dislocation lines. This is in contrast with defect locations reported for MgO insulating film where defects form preferentially at sites like steps, corners, and kinks [43]. Also, we note that most of the observed defects are single atom vacancies. A few cases of di-atomic or tri-atomic vacancies can be found.

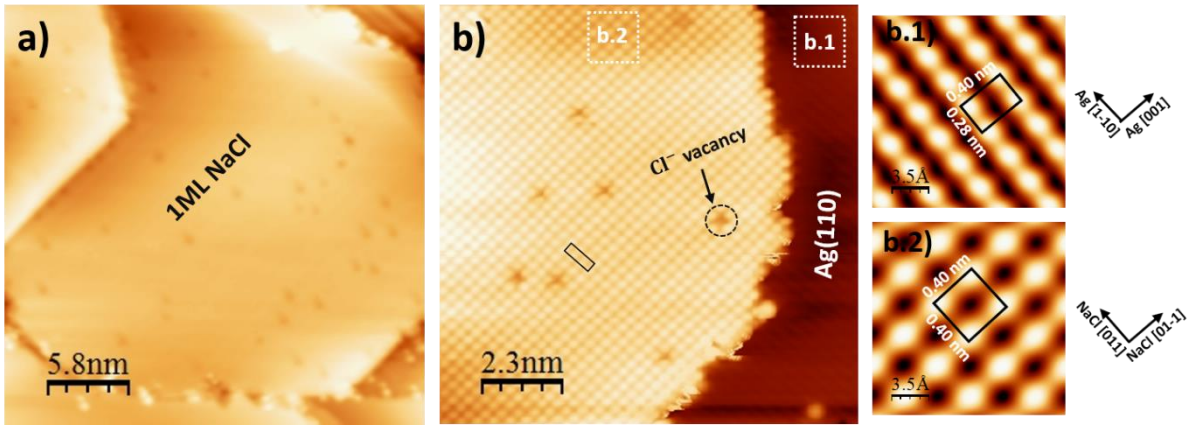

Figure 2. (a) STM topography (28.9 x 28.9 nm², U = -1 V , I = 0,4 nA) of 1ML NaCl film imaged after LEED surface analysis (electron exposure) which exhibits dark holes with high defect density; (b) Well-resolved STM image (11.6 x 11.6 nm², U = -0,6 V, I = 0,4 nA) showing Cl^- ions and Cl^- vacancies (black dashed circle) presented by protrusions and depressions, respectively. The superstructure periodicity (4x1) is presented by the rectangular unit cell with black line; b.1) Atomically resolved STM image of Ag(110) surface (17.5 x 17.5 Å², U = -0.04 V, I = 2.5 nA), the unit cell is indicated by black rectangle; b.2) Atomically resolved STM image of NaCl island (17.5 x 17.5 Å², U = -0.2 V, I = 0.7 nA), the unit cell is indicated by black square.

Figure 3 shows STM images taken prior to LEED surface analysis. Here, no NaCl surface defects were observed. This reveals that the high defect density observed in **Figure 2.a** is due to defect vacancies created by LEED electron irradiation. Similar NaCl defects have been found when using different experimental techniques such as electron energy loss spectroscopy (EELS) [18] or by bringing an STM tip into contact with the surface [44]. Since only the chlorine ions are imaged as bright spots in STM when using a metallic STM tip [45], the defects shown in **Figure 2.b** can be attributed to empty Cl vacancies. These defects appear as a simple hole in the NaCl surface, because they are simple cavities in the topmost NaCl(100) plane from a structural point of view.

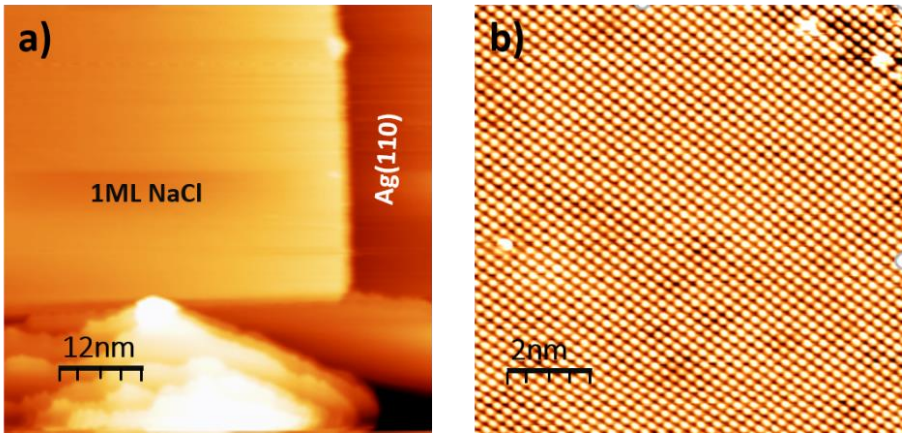

Figure 3. (a) STM topography (60 x 60 nm², U = -0.9 V , I = 1.2 nA) of 1ML NaCl film imaged prior to LEED surface analysis (electron exposure) showing a flat defect free NaCl island; (b) Atomically resolved STM image (10 x 10 nm², U = -0.6 V, I = 0.4 nA) recorded from the NaCl island of (a).

Figure 4 shows a detailed atomic resolution topography of a NaCl surface with a defect, presented in a standard 2D (**Figure 4.a**) and a pseudo 3D (**Figure 4.b**) representation for better visibility. The line profile in **Figure 4.c** corresponds to black line depicted in the STM image (**Figure 4.a**). The line profile clearly shows that the NaCl layer incomplete, *i.e.*, a Cl ion is missing, which leads to the appearance of a dark hole. The line scan also shows that the lattice defect has the form of a depression 70 pm deep and 0.4 nm diameter. The distance between the first neighbor protrusions of 0.4 nm corresponds to the distance between Cl ions in the NaCl (100) film. The depth of the dark depression is 70 pm, which is close to the measured apparent height of 1ML NaCl thin film [8]. This suggests that single-atom vacancy defects on NaCl can form even on the first layer.

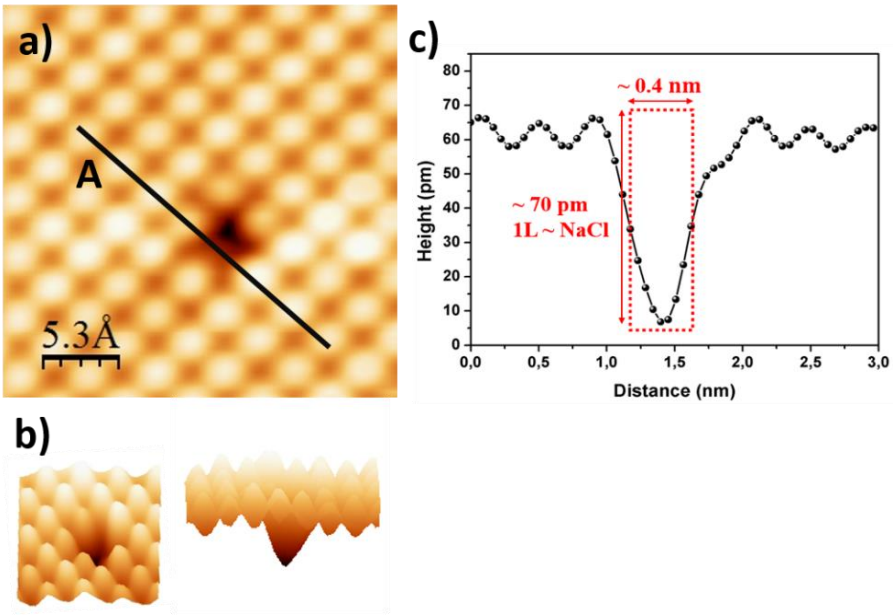

Figure 4. a) Atomically resolved STM topography (26.5 x 26.5 Å², U = -0.6 V, I = 0.6 nA) showing square symmetry of NaCl film with dark single Cl vacancy; b) Pseudo 3D representation of the NaCl surface defect for better visibility; c) line profile (A) taken across the vacancy showing an example of the defect dimensions.

In order to further investigate the effect of LEED electron irradiation on the NaCl thin film, we show in **Figure 5** a typical (AES) spectra of Ag(110) surface before and after deposition of 1 ML of NaCl. We used AES mainly to check the cleanliness of the substrate and investigate the surface chemical composition. The first spectrum (black line) presents the characteristic spectrum of Ag (MNN) collected from the clean Ag(110) surface. It shows peaks at 365 eV, 351 eV and secondary peaks at 302 eV, 260 eV [46]. After NaCl deposition (blue line), the Cl (LVV) peak appears at 181 eV. We can also observe that the silver Auger peak is attenuated after NaCl deposition. This attenuation is due to the loss of electrons travelling through the NaCl layer. Now, after electron irradiation of the NaCl film using the LEED during 10 min at an electron energy of 63 eV, we observe that the Ag signal slightly increases, while the Cl signal decreases. We should note that we were not able to detect the Na Auger peak in the spectrum in **Figure 5**. This is because the Na Auger peak is located at higher energy (KLL transition around 990 eV) and the peak intensity of Na is four times smaller than the peak intensity of Cl [46]. Note that the electron mean free path depends on the incident electron energy which is quite different for LEED (48 & 63 eV) compared to AES (3 keV). Low energy electrons (50 eV) can induce quite efficiently chemical transformations of thin self-assembled molecular layers [47].

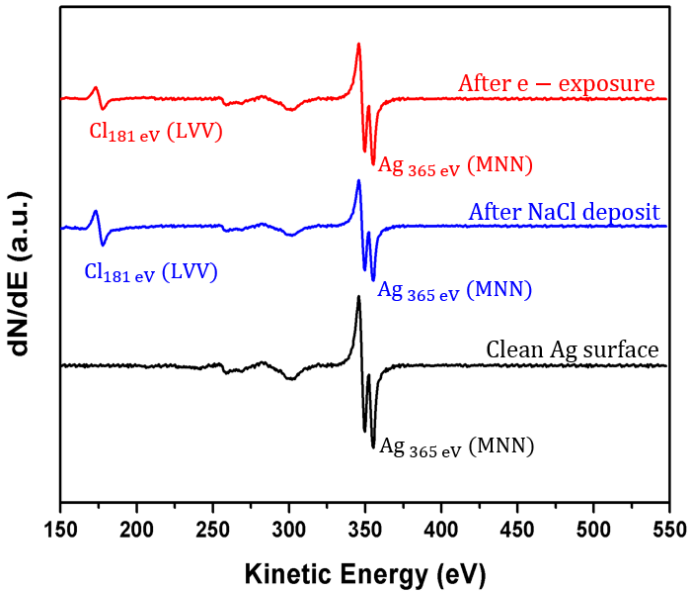

Figure 5. Differential AES spectra collected for: clean Ag(110) surface (black line), After deposition of 1ML NaCl (blue line) followed by electron bombardment (red line) during 10 min at 63 eV electron energy.

3.2. DFT Calculations

In this section we present the DFT results obtained for a defect-free and a defective NaCl layer adsorbed on the metallic Ag(110) surface. To model the Ag(110) surface, we created a 5-layer slab. We used 22 Å of vacuum between slabs in the z direction (perpendicular to the surface). Each Ag layer is composed of 12 atoms in a 4 x 3 surface unit cell giving a total of 60 atoms for the whole Ag(110) surface. The bulk lattice constant for Ag was found to be 4.154 Å and 4.147 Å, when using PBE and optB88, respectively. Once the slab was built, we optimized the Ag substrate and the NaCl film separately before depositing the adsorbate (NaCl) on the substrate (Ag). We keep the bottom two layers of the Ag surface fixed at their bulk-truncated positions and allowed the rest of the NaCl/substrate system to relax. The adhesion energy of the insulating NaCl film to the Ag metal surface is defined as:

$$E_{adhesion} = -(E_{NaCl/Ag(110)} - E_{NaCl} - E_{Ag(110)})/S \quad (1)$$

where S is the surface area of the substrate in Å^2. A positive adhesion energy implies a bound interface.

For the free standing NaCl(100) monolayer, the lattice parameter given by the Cl-Cl (Na-Na) nearest neighbors is 3.995 Å and 3.943 Å for PBE and OptB88, respectively, with the Cl anions and Na cations in a flat configuration. Upon NaCl adsorption, a lattice matching between the

NaCl ad-layer and the Ag(110) surface is obtained with a compression of 2.0% for PBE and 0.8% for OptB88 in the Ag[1-10] direction. However, along the Ag[001] direction, there is an expansion in the NaCl layer corresponding to 4.0% for PBE and 5.0% for OptB88. This compression and expansion corresponds to a NaCl:Ag matching of 3:4 and 1:1 along the [1-10] and [001] Ag directions, respectively, as shown in **Figure 6**. Therefore, when NaCl over-layer is placed on the Ag surface, the unit cell contains 3 NaCl pairs in agreement with the experimental LEED observation.

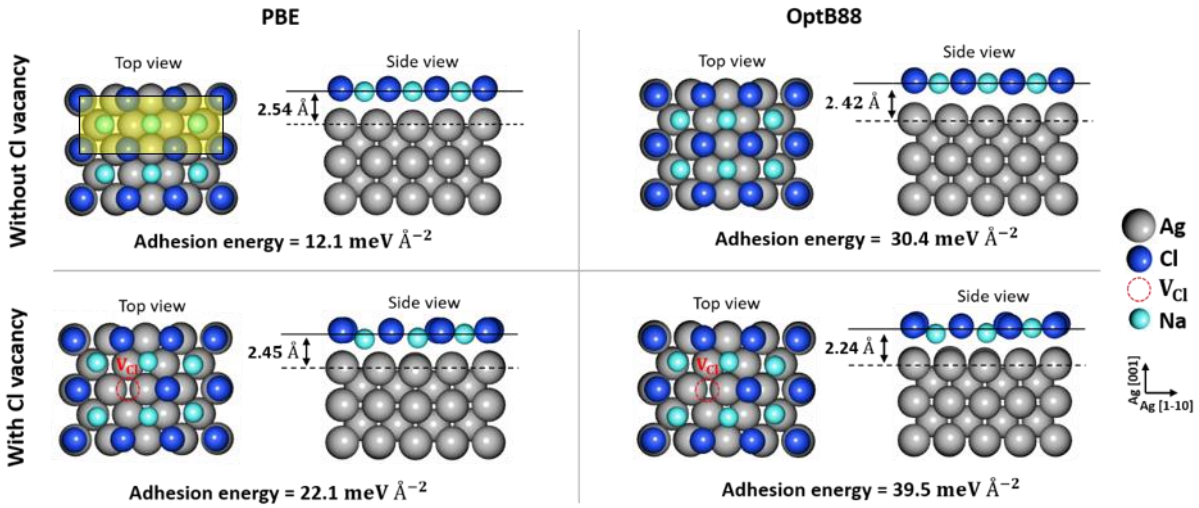

Figure 6. Computed structures and adhesion energies of defect-free and defective 1ML NaCl/Ag(110) as calculated using PBE and OptB88 functionals. Grey, blue and green spheres represent the Ag, Cl and Na atoms, respectively. The red dashed circle indicates the Cl vacancy. The Ag crystallographic directions correspond to the top view model. The superstructure periodicity (4x1) is presented by the highlighted rectangular unit cell which corresponds to a NaCl:Ag matching of 3:4 and 1:1 along the [1-10] and [001] directions.

Table 1 summarizes the adhesion energies and the distances obtained from the geometry optimization of defect-free and defective NaCl/Ag(110). From this table we can conclude for both systems a low adhesion energy for PBE as compared to OptB88. When accounting for the van der Waals effects, there is an increase in the adhesion energy between NaCl film and the metallic Ag substrate from 12.1 meVÅ^{-2} to 30.4 meVÅ^{-2} for the NaCl film without Cl vacancy and from 22.1 meVÅ^{-2} to 39.5 meVÅ^{-2} for NaCl film with a single Cl vacancy. These results confirm the importance of considering dispersion forces for ionic/metal systems. We note also that for defect-free NaCl, the Cl-Na inter-layer separation is 0.26 Å for both PBE and OptB88.

For the large unit cell used in the present study, as opposed to the one used in our previous study [8], there is a corrugation of about 0.10 Å for PBE and 0.17 Å for OptB88. The Na ions sit at nearly the same height above the surface. The average height separation between the Na plane and the Cl plane is 0.28 Å and 0.32 Å, for PBE and OptB88 respectively. When a Cl vacancy is created, the Na ions near the vacancy move towards the Ag plane by as much as 0.2Å for both PBE and OptB88, while the Cl ions near the vacancy move upwards away from the Ag plane by about 0.05-0.07 Å for both PBE and Optb88. For our unit cell we found a reduction in the difference in height between the average height of the Na plane and the top Ag plane. The height difference changed from 2.54 Å (2.42Å) to 2.45Å (2.24Å) when the vacancy is created for PBE (OptB88). Again, for the present cell, the charge transfer (from the NaCl film to the Ag substrate) is enhanced when the vacancy is created, from $0.45e^-$ to $1.14e^-$ for PBE and from $0.63e^-$ to $1.25e^-$ for OptB88.

Table 1. Adhesion energies calculated for 1ML NaCl/Ag(110) with and without Cl vacancy. Charge transfer between NaCl layer and Ag(110) surface. The interface distance $D_{NaCl/Ag}$ is defined as the distance between the average vertical position of the Ag top layer atoms and that of the Na plane.

Surface NaCl/Ag(110)	Functional Method	Adhesion Energy ($meV\text{Å}^{-2}$)	Charge Transfer (e) to Substrate	$D_{NaCl/Ag}$(Å)
Without Cl vacancy	PBE	12.1	0.45	2.54
Without Cl vacancy	OptB88	30.4	1.14	2.42
With Cl vacancy	PBE	22.1	0.63	2.45
With Cl vacancy	OptB88	39.5	1.25	2.24

Figure 7 shows a comparison between experimental and simulated STM images of clean Ag(110), defect free NaCl/Ag(110) and defective NaCl/Ag(110) surfaces. The simulated STM images showing the rectangular and square symmetries of Ag(110) and NaCl(100) surfaces, respectively, are in good agreement with the experimental STM topographies. From the structural model used for the calculations, we confirm that the imaged bright spots present the Cl ions, which is consistent with previous work [14]. For the defective NaCl layer, the

calculated STM image shows the Cl vacancy as depression which similar to the experimental observation.

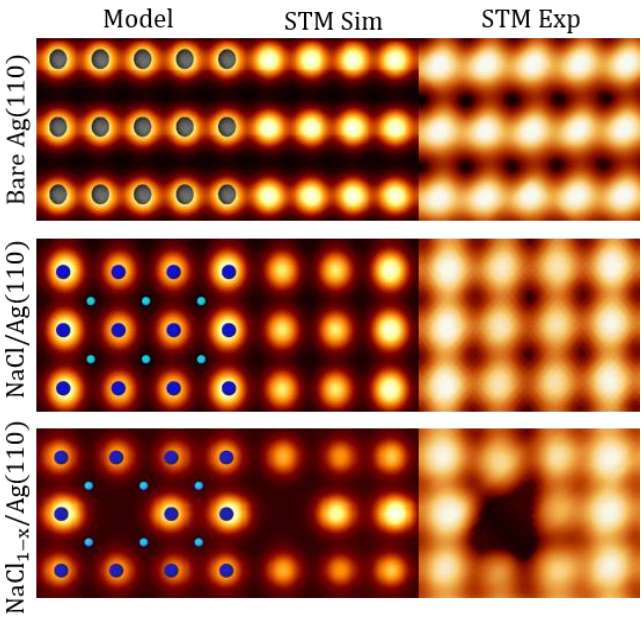

Figure 7. A comparison between simulated and experimental STM images of clean Ag(110) substrate (top image), defect-free NaCl monolayer deposited on Ag(110) (middle image) and NaCl monolayer with single Cl vacancy deposited on Ag(110) (bottom image). The related structural model for each system is given (left). The simulated STM images are taken at constant height mode with U = -1 V and an STM tip 3.0 Å above the average top layer of the scanned surface. Grey, dark blue and light blue corresponds to Ag, Cl and Na atoms, respectively.

4. Conclusion

In this work we present a combined experimental and computational study of Cl vacancy defects on NaCl thin film grown on Ag(110) metal surface. First, we show the formation of Cl vacancy defects due to electron-stimulated desorption with LEED beam during surface analysis at 48 eV. The topographic signature of these defects is imaged using STM showing the Cl vacancies as depressions on the NaCl surface. Furthermore, our STM simulation by DFT confirms the STM measurements. Comparing the adhesion of defect free NaCl and defective NaCl monolayers on Ag(110) surfaces, we found an increase of charge transfer between the NaCl layer and the Ag substrate due to the presence of Cl holes on the surface, and a decrease of NaCl spacing in the case of the defective layer. The increase in charge transfer may also be due to the Na atoms, which move closer to the Ag surface when the Cl vacancies are created. Overall, atomic vacancies can significantly influence the surface chemical reactivity,

controlling the density and nature of these defects should be beneficial for the applications of insulators in nano-scale devices [48, 49].

Notes

The authors declare no competing financial interest.

Acknowledgements

This work is supported by a public grant overseen by the French National Research Agency (ANR) as part of the "Investissements d'Avenir" program (Labex NanoSaclay, reference: ANR-10-LABX-0035). A.K. acknowledges support from the U.S. Department of Energy Basic Energy Science under contract no. DE-FG02-11ER16243. This research used resources of the National Energy Research Scientific Computing Center (NERSC), which is supported by the Office of Science of the U.S. Department of Energy, and the STOKES computational facility at the University of Central Florida.

References

[1] Repp J, Meyer G, Stojković S M, Gourdon A and Joachim C 2005 *Phys. Rev. Lett.* **94** 026803

[2] Swart I, Sonnleitner T, Niedenführ J and Repp J 2012 *Nano letters* **12** 1070-1074

[3] Repp J, Meyer G, Olsson F E and Persson M 2004 *Science* **305** 493-495

[4] Olsson F E, Paavilainen S, Persson M, Repp J and Meyer G 2007 *Phys. Rev. Lett.* **98** 176803

[5] Quertite K, Enriquez H, Trcera N, Tong Y, Bendounan A, Mayne A J, Dujardin G, Lagarde P, El Kenz A, Benyoussef A and Dappe Y J 2021 *Adv. Funct. Mater.* **31** 2007013

[6] Bombis C, Kalashnyk N, Xu W, Lægsgaard E, Besenbacher F and Linderoth T R 2009 *Small* **5** 2177-2182

[7] Pivetta M, Patthey F, Stengel M, Baldereschi A and Schneider W D 2005 *Phys. Rev. B* **72** 115404

[8] Quertite K, Lasri K, Enriquez H, Mayne A J, Bendounan A, Dujardin G, Trcera N, Malone W, El Kenz A, Benyoussef A and Kara A 2017 *J. Phys. Chem. C* **121** 20272-20278

[9] Repp J, Meyer G and Rieder K H 2004 *Phys. Rev. Lett.* **92** 036803

[10] Karacuban H, Koch S, Fendrich M, Wagner T and Möller R 2011 *Nanotechnology* **22** 295305

[11] Lauwaet K, Schouteden K, Janssens E, Van Haesendonck C and Lievens P 2012 *J. Phys. Condens. Matter.* **24** 475507

[12] Sun X, Felicissimo M P, Rudolf P and Silly F 2008 *Nanotechnology* **19** 495307

[13] Aït-Mansour K, Bielmann M, Gröning O, Ruffieux P, Fasel R and Gröning P 2006 *App. Surf. Sci.* **252** 6368-6374

[14] Husseen A, Le Moal S, Oughaddou H, Dujardin G, Mayne A and Le Moal E 2017 *Phys. Rev. B* **96** 235418

[15] Friedenberg A and Shapira Y. 1979 *Sur. Sci.* **87** 581-594

[16] Paparazzo E and Zema N 1997 *Surf. Sci.* **372** L301-L308

[17] Shapira Y and Friedenberg A 1980 *Int. J. Mass. Spectrom.* **36** 9-17

[18] Zielasek V, Hildebrandt T and Henzler M 2000 *Phys. Rev.B* **62** 2912

[19] Florez E, Fuentealba P and Mondragón F 2008 *Catal. today* **133** 216-22

[20] Sha Z D, Pei Q X, Zhang Y Y and Zhang Y W 2016 *Nanotechnology* **27** 315704

[21] Politano A, Chiarello G, Kuo CN, Lue CS, Edla R, Torelli P, Pellegrini V, Boukhvalov DW 2018 *Adv. Funct. Mater.* **28** 1706504.

[22] Matsunaka D, Rodulfo ET and Kasai H 2005 *Solid state commun.* **134** 355-60

[23] Quertite K, Zaari H, Ez-Zahraouy H, El Kenz A, Oughadou H and Benyoussef A 2017 *Curr. Appl. Phys.* **17** 1271-8

[24] Stengel M, De Vita A and Baldereschi A 2003 *Phys. Rev. lett.* **91** 166101

[25] Hynninen T, Cabailh G, Foster A S and Barth C 2013 *Sci. Rep.* **3** 1-6

[26] Repp J, Meyer G, Paavilainen S, Olsson F E and Persson, M 2005 *Phys. Rev. let.* **95** 225503

[27] Steurer W, Gross L and Meyer G 2014 *App. Phys. Lett.* **104** 231606

[28] Kresse G and Furthmüller J 1996 *Phys. Rev. B: Condens. Matter Mater. Phys.* **54** 11169−11186

[29] Kresse G and Furthmüller J 1996 *Comput. Mater. Sci.* **6** 15−50

[30] Perdew J P, Burke K and Ernzerhof M 1996 *Phys. Rev. Lett.* **77** 3865−3868

[31] Blöchl P 1994 *Phys. Rev. B: Condens. Matter Mater. Phys.* **50** 17953−17979

[32] Kresse G and Joubert D 1999 *Phys. Rev. B: Condens. Matter Mater. Phys.* **59** 1758−1775

[33] Klimeš J. and Michaelides A 2012 *J. Chem. Phys.* **137** 120901

[34] Yildirim H, Greber T and Kara A 2013 *J. Phys. Chem. C* **117** 20572−20583

[35] Matos J, Yildirim H and Kara A 2015 *J. Phys. Chem. C* **119** 1886−1897

[36] Yildirim H and Kara A 2013 *J. Phys. Chem. C* **117** 2893−2902

[37] Yildirim H, Matos J and Kara A 2015 *J. Phys. Chem. C* **119** 25408−25419

[38] Matos J, Rojas T, Yildirim H and Kara A 2014. *J. Chem. Phys.* **140** 144703

[39] Monkhorst H J and Pack J D 1976 *Phys. Rev. B* **13** 5188−5192

[40] Tang W, Sanville E and Henkelman G 2009 *J. Phys. Condens. Matter.* **21** 084204

[41] Henkelman G, Arnaldsson A and Jónsson H 2006 *Comput. Mater. Sci.* **36** 354-360

[42] Tersoff J and Hamann D R 1985 *Phys. Rev. B* **31** 805

[43] Sterrer M, Heyde M, Novicki M, Nilius N, Risse T, Rust H P, Pacchioni G and Freund H J 2006 *J. Phys. Chem. B* **110** 46-9

[44] Li Z, Chen H Y T, Schouteden K, Lauwaet K, Janssens E, Van Haesendonck C, Pacchioni G and Lievens P 2015 *ACS nano* **9** 5318-5325

[45] Li Z; Schouteden K, Iancu V, Janssens E, Lievens P, Van Haesendonck C and Cerdá J I 2015 *Nano Research* **8** 2223-2230

[46] Davis L E, MacDonald N C, Palmberg P W, Riach G E and Weber R E 1976 Handbook of Auger Electron Spectroscopy. *Physical Electronics Division*

[47] Houplin J, Dablemont C, Sala L, Lafosse A and Amiaud L 2015 *Langmuir* **31** 13528-13534

[48] Illarionov Y Y, Knobloch T, Jech M, Lanza M, Akinwande D, Vexler M I, Mueller T, Lemme M C, Fiori G, Schwierz F and Grasser T 2020 *Nature Commun.* **11** 1-15

[49] Jain N, Durcan CA, Jacobs-Gedrim R, Xu Y and Yu B 2013 *Nanotechnology* **24** 355202